



50. Modeling and Control of Robots on Rough Terrain

Keiji Nagatani, Genya Ishigami, Yoshito Okada

In this chapter, we introduce modeling and control for wheeled mobile robots and tracked vehicles. The target environment is rough terrains, which includes both deformable soil and heaps of rubble. Therefore, the topics are roughly divided into two categories, wheeled robots on deformable soil and tracked vehicles on heaps of rubble.

After providing an overview of this area in Sect. 50.1, a modeling method of wheeled robots on a deformable terrain is introduced in Sect. 50.2. It is based on terramechanics, which is the study focusing on the mechanical properties of natural rough terrain and its response to off-road vehicle, specifically the interaction between wheel/track and soil. In Sect. 50.3, the control of wheeled robots is introduced. A wheeled robot often experiences wheel slippage as well as its sideslip while traversing rough terrain. Therefore, the basic approach in this section is to compensate the slip via steering and driving maneuvers. In the case of navigation on heaps of rubble, tracked vehicles have much advantage. To improve traversability in such challenging environments, some tracked vehicles are equipped with subtracks, and one kinematical modeling method of tracked vehicle on rough terrain is introduced in Sect. 50.4. In addition, stability analysis of such vehicles is introduced in Sect. 50.5. Based on such kinematical model and stability analysis, a sensor-based control of tracked vehicle on rough terrain is introduced in Sect. 50.6. Sect. 50.7 summarizes this chapter.

50.1 Overview	1268	50.2 Modeling of Wheeled Robot in Rough Terrain	1270
50.1.1 Modeling Deformable Terrain for Robots	1268	50.2.1 Dynamics of Mobile Robots	1270
50.1.2 Controlling Robots in Deformable Terrain	1268	50.2.2 Wheel–Terrain Interaction Mechanics	1271
50.1.3 Modeling and Controlling Robots in Heaps of Rubble	1269	50.2.3 Wheel Traction Performance	1273
		50.2.4 Model Uncertainty and Soil Parameter Identification	1273
		50.3 Control of Wheeled Robot in Rough Terrain	1274
		50.3.1 Slip–Compensated Path Follower	1274
		50.3.2 Steering and Driving Maneuvers	1275
		50.4 Modeling of Tracked Vehicle on Rough Terrain	1276
		50.4.1 Parameterization of a Track	1277
		50.4.2 Contact with a Single Point in the Terrain Surface	1277
		50.4.3 Contact with the Terrain Surface Represented by a Point Cloud	1277
		50.5 Stability Analysis of Tracked Vehicles	1278
		50.6 Control of Tracked Vehicle on Rough Terrain	1279
		50.6.1 Ground Detection and Trimming of the Scanned Data	1280
		50.6.2 Determination of Desired Posture	1280
		50.6.3 Determination of Desired Subtrack Positions	1280
		50.6.4 Stability Evaluation of Desired Pose	1281
		50.6.5 Stabilization of Desired Pose	1281
		50.6.6 Position Control of Subtracks	1281
		50.7 Summary	1281
		Video–References	1281
		References	1282

50.1 Overview

50.1.1 Modeling Deformable Terrain for Robots

The category of rough terrain includes a variety of ground conditions. In the case of weak and fine gravel, the motion of a wheeled mobile robot becomes relatively complicated because the interaction mechanics of the wheel in a rough terrain differs from that of an indoor robot on a flat surface; a wheel on gravel has multiple point contact, and a wheel on loose soil has a surface contact that deforms the soil around the wheel.

There has been a large amount of research on robot mobility analysis in the military community [50.1, 2]. These studies have primarily focused on empirical analyses of large vehicles (i. e., gross vehicle weights of several tons). The mobility analyses of small mobile robots that consider the interaction mechanics of a slipping wheel on rough terrain have also been investigated. Additionally, a multibody system simulation for the longitudinal slip of tires with respect to the tire–soil interaction has been demonstrated [50.3]. A dynamic interaction model, denoted as soil contact model (SCM), has been developed to provide the dynamics of a plastically deformable surface using an elevation grid, as well as to consider the multipass effect of wheels, shown in Fig. 50.1 [50.4]. Recently, multibody dynamics toolkit, such as Vortex (VIDEO 184), can be used to simulate terrain reaction forces for mobility analyses of mobile robots [50.5].

Recently, terramechanics [50.6] has been widely used in applications such as off-road UGVs (unmanned ground vehicles) [50.7, 8] and planetary rovers on Mars. A fundamental requirement for such off-road mobile robots is to maintain a traversing capability in rough

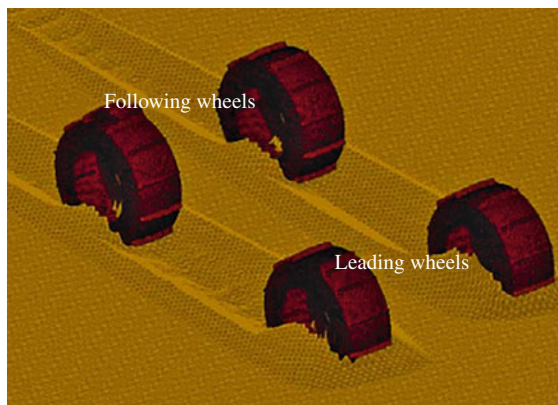


Fig. 50.1 Dynamics of a plastically deformable surface in consideration with the multipass effect of wheels (after [50.4])

terrain composed of loose sand, mud, pebbles, etc. One typical issue in such an environment is wheel slippage, which is generated because of the soil deformation at the wheel–terrain contact patch. Wheel slippage often degrades the mobility performance of the robot because some amount of tractive power from a driving actuator is consumed by the soil deformation. Furthermore, the wheel slippage induces vehicle sideslip, which is an additional disturbance for the motion control of a wheeled robot. Figure 50.2 shows one typical example of lateral- and side-slip situation of a wheeled mobile robot in rough terrain. One typical example of terramechanics-based modeling of rough terrain is described in Sect. 50.2. Recently, a study of terradynamics of legged locomotion was proposed for traversal in granular media in [50.9] and is shown in VIDEO 186.

50.1.2 Controlling Robots in Deformable Terrain

A wheeled robot often experiences wheel slippage as well as vehicle sideslip while traversing rough terrain. This degrades the motion control performance of the robot, i. e., a robot could deviate from the path to be followed or a wheel may get trapped in loose soil. Therefore, a control scheme that can derive the appropriate steering/driving maneuvers is necessary for a wheeled robot to achieve traversability on a rough terrain and to manage any slippage problems that may arise.

A large number of studies related to the path-following control of mobile robots have been published. General information on path-following issues can be obtained from [50.10–12]. Rezaei et al. investigated an online path-following strategy combined with a simultaneous localization and mapping (SLAM) algorithm for a car-like robot in outdoor environments [50.13].



Fig. 50.2 Lateral- and side-slip situation of wheeled mobile robot

Coelho and *Nunes* et al. proposed a Kalman-based active observer controller for the path-following of wheeled mobile robots [50.14]. *Helmick* et al. developed a path-following algorithm that included slip compensation by using visual odometry and a Kalman filter [50.15, 16]. The method was applied to the rocker-bogie configuration with six steerable wheels robot, shown in Fig. 50.3. In Sect. 50.3, a path-following control scheme for a four-wheeled mobile robot is introduced. The experimental validation of the control described in the section was reported in [50.17].

50.1.3 Modeling and Controlling Robots in Heaps of Rubble

In environments that involve heaps of rubble, such as an urban search and rescue situation, the approach for modeling and controlling robots is different from the afore mentioned methodology. To tackle such challenging environments, tracks are used to enhance the mobility of a robot in such environments because they have more contact with the terrain than wheels. Some tracked vehicles are equipped with active subtracks, and multitracks configuration enables the vehicle to get over relatively large steps. A typical geometrical model of tracked vehicles with subtracks is introduced in Sect. 50.4.

In case that the target rubble is stable, kinematic approaches are useful for navigation and control of the robot. In this case, stability analysis is very important. In classical stability analysis, the energy stability margin (ESM) proposed by *Messuri* and *Klein* was defined in terms of the potential energy of the robot [50.18]. *Hirose* assumed that increasing the robot's weight did not always contribute to its stability because it also increased the dynamic disturbance around its center of gravity. Therefore, he proposed the normalized ESM

(NESM), in which the robot's weight was normalized [50.19]. For this criterion, the NESM is used to evaluate the stability of a robot on the basis of the vertical distance between the initial and largest heights of the center of gravity during a rollover. Recently, *Tubouchi*'s group proposed a method to control tracked vehicles exposed to random steps [50.20] (Fig. 50.4). An artificial uneven environment is random steps, arranged with different lengths of squared timbers. It also appears in VIDEO 189. This environment is used to evaluate the performance for urban search and rescue robots [50.21]. The basic objective is to maintain the maximal stability of the robot at every step of its path in the random step field. The earlier-given topic relating to stability analysis is introduced in Sect. 50.5. Another approach for stability analysis of tracked vehicles-based NESM was reported in [50.22].

To evaluate the stability of vehicles, terrain detection is an important technology. Therefore, many robotics researchers have focused on the terrain mapping, particularly based on the SLAM, described in Chap. 46, and machine learning. LIDAR (light detection and ranging) and stereo cameras are widely used for the terrain mapping (Sect. 22.3). *Vandapel* et al. proposed a classification method of three-dimensional (3-D) point cloud data on the basis of its geometrical features [50.23], and *Lacaze* et al. demonstrated a method of finding a path in heavy grasses [50.25]. To improve the LIDAR-based mapping, *Ohno* et al. proposed a method to obtain thin objects such as nets, poles, and wires [50.26]. Figure 50.5 shows a mapping result at an outdoor rough terrain.

If the rubble is unstable, modeling the machine-rubble interaction is very complicated. One challenging



Fig. 50.3 Rocky 8: rocker-bogie configuration with six steerable wheels robot

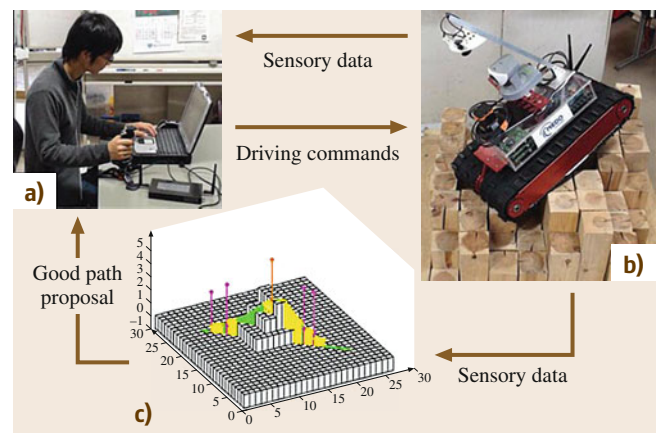


Fig. 50.4a-c Teleoperated system of tracked vehicle. It consists of (a) a remote operation station, (b) a mobile robot platform, and (c) path planner that maintain the maximal stability of the robot (after [50.20])

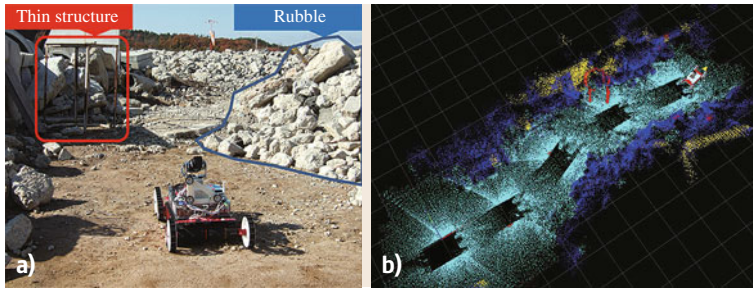


Fig. 50.5a,b Classification of outdoor rubble data. **(a)** Target field: Hyogo Prefectural Emergency Management and Training Center, and **(b)** classified result for traversal (after [50.23])

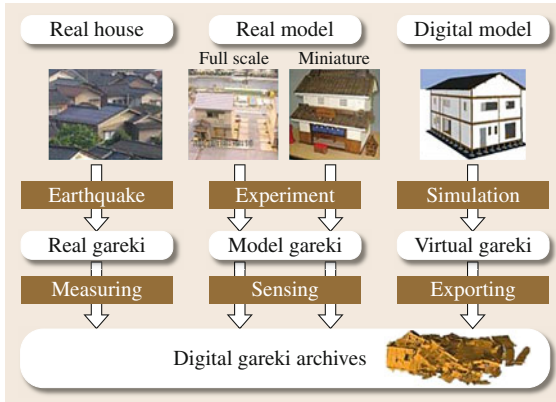


Fig. 50.6 Approaches for gareki data acquisition (after [50.24])

approach to modeling rubble is called gareki (rubble in Japanese) engineering [50.27, 28]. The model includes not only the structure data, but also the internal force of each gareki element. To obtain the data, they proposed to use information about the following, as shown in Fig. 50.6: (1) a real-collapsed building, (2) artificial full- and miniature-scale col-

lapsed buildings, and (3) a simulated virtual digital building. Their research aims to eventually apply the gareki model for the control of mobile robots and rescue missions.

The sensor-based method is another approach for controlling robots in unstable rubbles. Such robots often have multiple tracks connected by joints to maneuver over natural/artificial steps, bumps, and stairs. Some are equipped with passive joints [50.29], but many are equipped with active joints [50.30]. Multitrack configurations enable the vehicle to maneuver over a step that is higher than the radius of the tracks. To enable such motion, a sensor-based method is proposed to control the multitracks. The robot moves and detects the surface shape of the ground continuously, and it changes the configuration of the subtracks based on the surface information. Once the surface of the ground is deformed by the traversal of the robot, the subtracks adapt quickly. A representative example for the control of robots in unstable rubble is shown in Sect. 50.6. Another sensor-based approach is to use force-feedback from contact points. Inoue et al., embedded force sensors in their subtracks to obtain the contact force, and changed the configuration of the subtracks [50.31].

50.2 Modeling of Wheeled Robot in Rough Terrain

This section introduces a mechanics of wheeled mobile robot in rough terrain, particularly focusing on a modeling of wheel–terrain interaction.

50.2.1 Dynamics of Mobile Robots

Figure 50.7 depicts a schematic illustration of a dynamic model for a wheeled mobile robot. The robot is modeled as an articulated multibody system. The equation of motion for the robot is numerically given by

$$\mathbf{H} \begin{pmatrix} \dot{\mathbf{V}}_b \\ \ddot{\mathbf{q}} \end{pmatrix} + \mathbf{C} + \mathbf{G} = \begin{pmatrix} \mathcal{F}_b \\ \boldsymbol{\tau} \end{pmatrix} + \mathbf{J}^T \mathcal{F}_e, \quad (50.1)$$

where the symbols have the following meanings: \mathbf{H} : inertia matrices composed of multibody of the robot, \mathbf{C} : velocity depending term, \mathbf{G} : gravity term, \mathcal{V}_b : translational and angular velocities of the vehicle, \mathbf{q} : joint angles (such as wheel rotation and steering angles), \mathcal{F}_b : forces and moments at the centroid of the vehicle body, $\boldsymbol{\tau}$: torques acting at each joint (driving/steering torques), \mathbf{J} : Jacobian matrix, \mathcal{F}_e : external forces and moments acting at the centroid of each wheel, namely

$$f_{ij} (i = \{r, l\}, j = \{r, m, f\}).$$

The dynamic motion of the robot with given traveling and steering maneuvers are numerically obtained

by successively solving (50.1). Here, a key approach for the dynamic model is to incorporate a well-defined contact model into the equation of motion in order to calculate the external forces and torques at the contact patch between the wheel and terrain. Some recent works have reported dynamic simulation tools combined with the terramechanics wheel model: for example, [50.32, 33] for the NASA's rovers, and [50.4, 34] for the ExoMars.

50.2.2 Wheel–Terrain Interaction Mechanics

Terramechanics is a study focusing on the mechanical properties of natural rough terrain and its response to off-road vehicle, specifically the interaction between wheel/track and soil. In 1960s, *Bekker* developed a classical terramechanics with many of the key concepts related to vehicle–terrain response, such as a well-known pressure-sinkage equation and shear stress model [50.35, 36]. Wong developed a comprehensive procedure for predicting the performance of both driven and towed wheels [50.37–39]. The procedure calculates the wheel mechanics with applying the stress distribution model beneath the wheel.

Terramechanics-based approach for vehicle–terrain mechanics includes mainly three methodologies [50.40, 41]: (1) Analytical approach, (2) empirical approach, and (3) numerical approach.

The analytical approach is based on a theoretical model for vehicle–terrain interactions along with experimental model validation. The empirical method is to utilize a practical measurement of soil strength

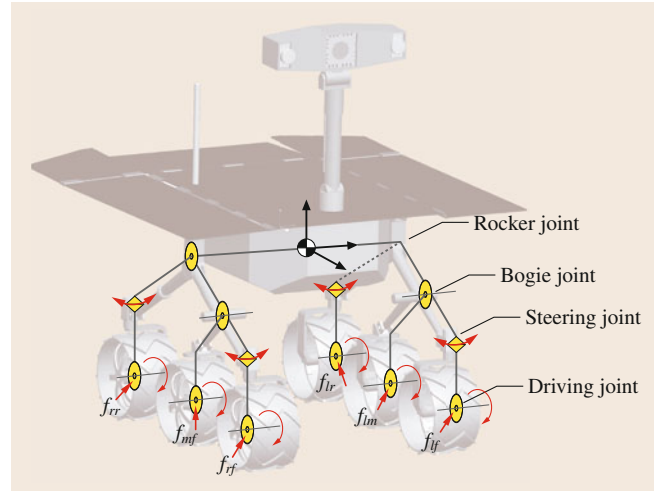


Fig. 50.7 Dynamic model of wheeled mobile robot

by a specialized apparatus in order to estimate vehicle traversability on weak/rough terrain. The numerical method includes the finite element method (FEM) and discrete element method (DEM) that models soils as vast numbers of multiple particles and simulates each particle's behavior while accounting vehicle–terrain interaction [50.42–44].

This subsection focuses on the analytical method and introduces a typical interaction model of rigid wheel on deformable terrain (Fig. 50.8). It should be noted that Chap. 55.3.13 also addresses the wheel traction mechanics in detail, and therefore, the following subsection recalls some key equations in order to dis-

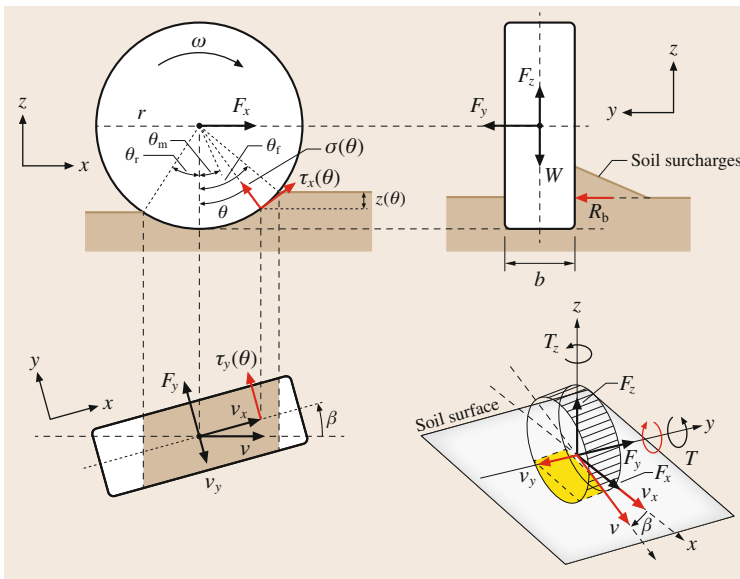


Fig. 50.8 Wheel–terrain contact model

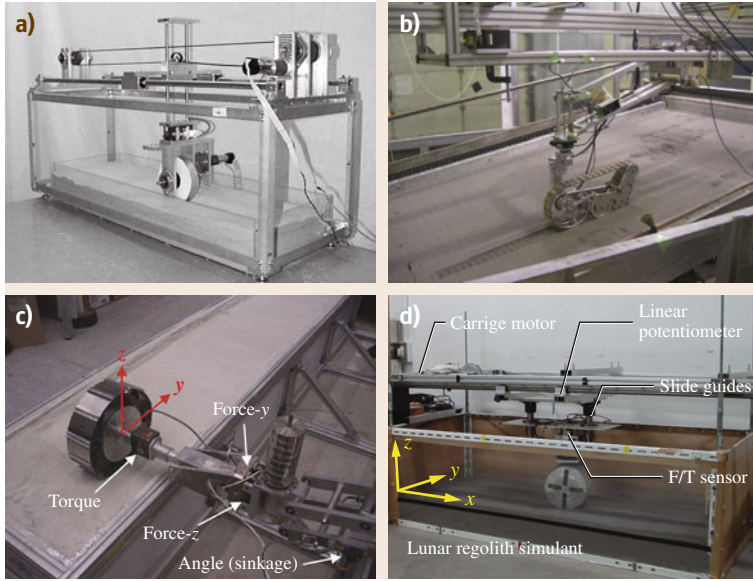


Fig.50.9a–d Single wheel test beds for experimental validation of terramechanics models. **(a)** Single wheel test bed at MIT (after [50.45]), **(b)** Single track test bed at JAXA (after [50.46]), **(c)** Single wheel test bed at DLR (after [50.47]), **(d)** Single wheel test bed at Tohoku University. (after [50.48])

cuss a wheel traction characteristics on rough terrain, soil parameter identification, and model uncertainty.

Wheel Slippage

Wheel slippage is generally observed when a robot travels on loose soil. Also, the wheel will slip in the lateral direction while the robot steering or traversing on sloped terrain. The slip ratio (i. e., slip in the longitudinal direction of wheel travel) is defined as a function of the longitudinal traveling velocity of the wheel v_x and the circumferential velocity of the wheel $r\omega$, where r is the wheel radius and ω represents the angular velocity of the wheel [50.37]

$$s = \begin{cases} (r\omega - v_x)/r\omega & (|r\omega| \geq |v_x| : \text{driving}) , \\ (r\omega - v_x)/v_x & (|r\omega| < |v_x| : \text{braking}) . \end{cases} \quad (50.2)$$

The slip ratio assumes a value in the range from -1 to 1 .

The slip in the lateral direction of the wheel is expressed by the slip angle β , which is defined as a function of v_x and the lateral traveling velocity v_y , as

$$\beta = \begin{cases} \tan^{-1}(v_y/v_x) & (v_x \neq 0) , \\ \text{sgn}(v_y) \cdot \pi/2 & (v_x = 0) . \end{cases} \quad (50.3)$$

Wheel Traction Forces

The wheel–terrain contact forces, including the drawbar pull F_x , side force F_y , vertical force F_z , and resistance torque T , are calculated as the integral of the normal

and shear stresses from the entry angle θ_f and the exit angle θ_r [50.38, 48]

$$F_x = rb \int_{\theta_r}^{\theta_f} \{ \tau_x(\theta) \cos \theta - \sigma(\theta) \sin \theta \} d\theta , \quad (50.4)$$

$$F_y = \int_{\theta_r}^{\theta_f} [rb\tau_y(\theta) + R_b \{r - z(\theta) \cos \theta\}] d\theta , \quad (50.5)$$

$$F_z = rb \int_{\theta_r}^{\theta_f} \{ \tau_x(\theta) \sin \theta + \sigma(\theta) \cos \theta \} d\theta , \quad (50.6)$$

$$T_x = r^2 b \int_{\theta_r}^{\theta_f} \tau_x(\theta) d\theta , \quad (50.7)$$

where $\sigma(\theta)$ is the normal stress, $\tau_x(\theta)$ and $\tau_y(\theta)$ are the shear stresses in the longitudinal or lateral direction. $z(\theta)$ is the wheel sinkage at an angle of θ , b is the wheel width, and R_b is the bulldozing resistance generated on a side wall of the wheel.

Experimental Validation

An experimental validation of the afore mentioned wheel–terrain interaction model is performed by the use of a single wheel test bed (Fig. 50.9), with varied state parameters such as soil or wheel slip conditions. A carriage velocity controlled relative to a wheel velocity realizes a wheel slip (or traction load) while measuring wheel traction forces, wheel

sinkage, and others. Experimental data obtained from the test bed are then compared with the values obtained from numerical simulation of the wheel traction model.

50.2.3 Wheel Traction Performance

The wheel–terrain model can be exploited for an evaluation of the mobility performance of a wheeled robot (i. e., traversability on sloped or deformable terrain [50.49, 50]). Such mobility evaluation technique is further valuable for the mobility system design in order to find a feasible wheel/track design that maximizes the traction performance for off-road locomotion under some specific constraints [50.46, 47, 51].

Ishigami et al. proposed a wheel traction diagram called a thrust–cornering characteristic diagram that determines the slope traversal criteria with respect to wheel slip conditions [50.17]. Figure 50.10 illustrates the relationship between the thrust and cornering forces of wheel on rough terrain, with varied slip ratios/slip angles. The thrust and cornering forces F_c and F_T are obtained by calculating the drawbar pull and side force

$$F_c = F_x \sin \beta + F_y \cos \beta, \quad (50.8)$$

$$F_T = F_x \cos \beta - F_y \sin \beta. \quad (50.9)$$

Considering the slope traversal scenario as shown in Fig. 50.11, the thrust–cornering characteristic diagram can draw the criteria with a minimum cornering force and thrust force required for a slope traversal: Case 1 as a traversal and uphill traveling, Case 2 as a straight-line traversal, and Case 3 as a traversal and downhill traveling. In addition, a robot decelerates or cannot move forward due to its negative thrust force. This diagram, for example, indicates that the slip ratio must exceed 0.6 in order to generate positive thrust force, and also, the cornering force varies primarily with the slip angle. Therefore, the diagram can determine the slope traversability on the basis of the corresponding slip-page, indicated by several characteristic curves on the diagram.

50.2.4 Model Uncertainty and Soil Parameter Identification

It should be noted that the classical terramechanics model has primarily developed for an application for large-heavy vehicles (hundreds/thousands kg weight). Therefore, several assumptions that may cause an inaccurate calculation of wheel traction performance of

the classical model would be omitted while exploiting the classical model to an analysis of small lightweight robot, resulting in an inaccurate calculation of wheel traction performance. The error due to the inadequate assumptions for the small-lightweight robot can be addressed by the following approaches: model improvement and uncertainty analysis of model parameters. It should be noted that the Bekker's pressure-sinkage model is assumed that the contact patch of wheel on deformable soil (circumferential section) is discretized

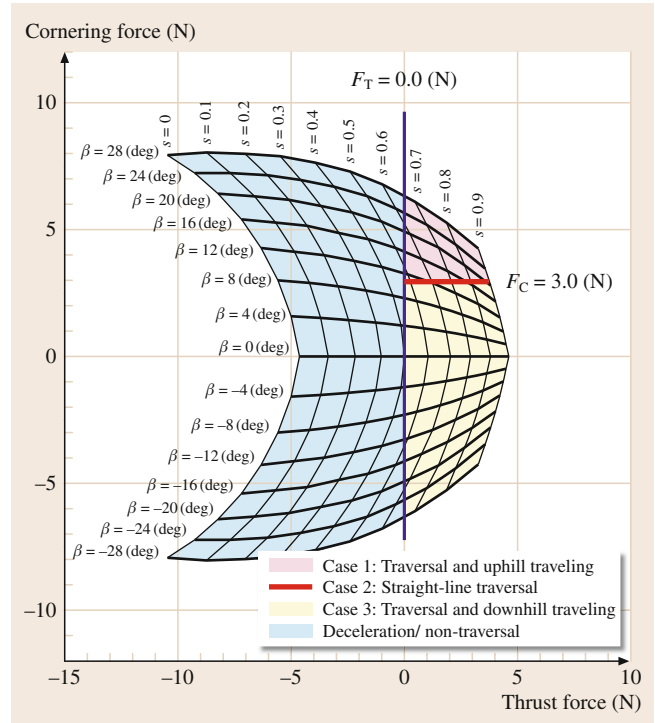


Fig. 50.10 Thrust–cornering characteristic diagram

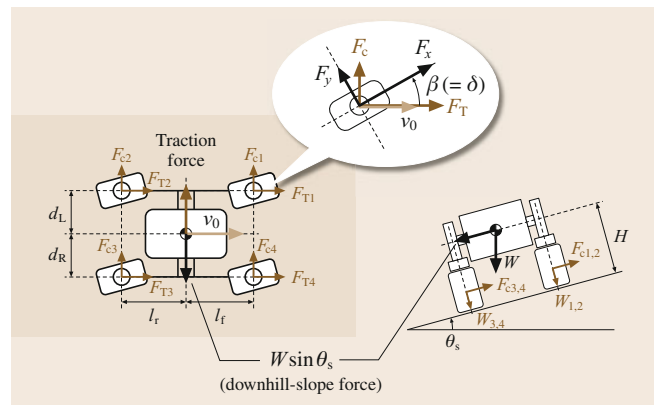


Fig. 50.11 Force balance on slope traversal

as a series of consecutive flat plate; however, *Bekker* noted [50.36]:

Predictions for wheels smaller than 20 inches in diameter become less accurate as wheel diameter decreases, because the sharp curvature of the loading area was neither considered in its entirety nor is it reflected in bevameter tests.

Also another research reported that the assumptions provide inaccurate prediction for vehicles with wheels diameter less than about 50 cm (approx.) and normal loading less than 45 N (approx.) [50.36].

Some researchers have tried to update/improve the classical terramechanics model that can be successfully applied to relatively light weight vehicles: For example, *Nagatani* et al. developed a direct measurement device for the normal stress distribution [50.52]. A wheel diameter dependent pressure-sinkage model has been proposed by [50.53]. *Senatore* and *Iagnemma* proposed

an improved approach for the calculation of shear deformation modulus [50.54].

Model parameters in the wheel–terrain interaction related to the soil properties are subject to uncertainties since their values would stochastically vary with location. Several researches have addressed the soil parameter identification: an on-line terrain parameter estimator with simplifying classical terramechanics equations was proposed by [50.55]; a modified nonlinear wheel–terrain interaction model for an identification of pressure-sinkage coefficient, internal friction angle, and shear deformation modulus [50.56]. Some recent works have also attempted to predict rover mobility even in uncertain conditions: a learning-based approach for slip-prediction and traversability analysis of a wheeled robot [50.57]; and a statistical method for mobility prediction of a robot with taking into account of terrain uncertainty [50.58].

50.3 Control of Wheeled Robot in Rough Terrain

This section introduces a control scheme for the wheeled robot that compensates wheel-and-vehicle slippages while following a given path is described.

A wheeled robot often experiences wheel slippages as well as vehicle sideslip while traversing in rough terrain, which degrades a performance of a motion control of the robot: i.e., a robot will deviate from a path to be followed, or a wheel might get stuck into loose soil. Therefore, a control scheme that can derive appropriate steering/driving maneuvers is necessary for a wheeled robot to achieve a rough terrain traverse and to manage any slippage problems.

A significant number of studies related to the path following control of mobile robot have been published. A general note for path following issues can be seen in [50.10–12]. *Rezaei* et al. investigated an online path following strategy combined with a simultaneous localization and mapping (SLAM) algorithm for a car-like robot in outdoor environments [50.13]. *Coelho* and

Nunes et al. proposed a Kalman-based active observer controller for the path following of wheeled mobile robots [50.14].

As noted before, a key issue of the path following on rough terrain is to compensate wheel-and-vehicle slippage. This subsection briefly introduces a slip-compensated path follower along with a derivation for steering and driving maneuvers for path following [50.15–17] which is shown in [VIDEO 188](#).

50.3.1 Slip-Compensated Path Follower

A two-dimensional path-following problem of a mobile robot is shown in Fig. 50.12. Here, a path following control generally performs to let the vehicle velocity v_0 coincide with the tangent of a given path such that the distance and orientation errors decrease to zero. However, once the vehicle experiences a sideslip with a certain amount of slip angle β_0 , the vehicle has an additional orientation error of β_0 even

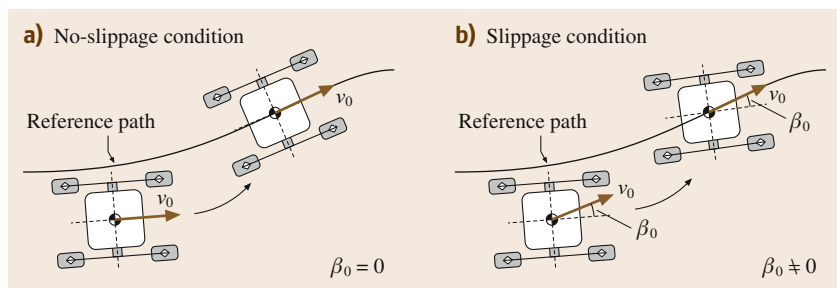


Fig. 50.12a,b Path following problem without (a) and with (b) slip angle of vehicle

when the vector of vehicle velocity completely follows the path (Fig. 50.12b).

The path follower basically derives a commanded robot velocity vector $(\dot{x}_{\text{cmd}}, \dot{y}_{\text{cmd}}, \dot{\theta}_{\text{cmd}})$ while the robot position (x_0, y_0, θ_0) and a reference path vector (x_p, y_p) are given. The slip-compensated path follower described here consists of two algorithms to achieve a path following task through high-slip environments.

First, the carrot heading algorithm determines the heading error of the robot θ_e , which is an angle calculated from the intersection of a circle centered on the robot coordinate with the desired path (Fig. 50.13):

$$\theta_e = \theta_d - \theta_0 \quad (50.10)$$

Here, θ_d is the desired heading angle which is a tangent angle on the intersection point and θ_0 is the robot heading angle. A large radius of the circle will generate a smooth motion of the robot while neglect a small feature of the path. A small radius will reduce the total path following error, but requires frequent heading changes for small path errors.

Once the heading error is determined, the slip-compensated path following algorithm executes the heading controller that calculates the commanded yaw rate of the robot $\dot{\theta}_{\text{cmd}}$ from the heading error θ_e and the yaw slip rate $\dot{\beta}_0$

$$\dot{\theta}_{\text{cmd}} = \frac{(K_1 \cdot \theta_e + K_2 \cdot \dot{\beta}_0)}{T_s}, \quad (50.11)$$

where K_1 and K_2 are the tuned controller gains, and T_s is the sampling period.

Note that the command for the linear velocity \dot{x}_{cmd} and \dot{y}_{cmd} are closely related to the maximum speed of the driving motors and the desired heading angle $\dot{\theta}_{\text{cmd}}$. Practically, these commands are accomplished by actuators of the robotic mobility system, namely steering and driving mechanisms. The following subsection describes the derivation of those steering and driving maneuvers that satisfies the heading controller command $\dot{\theta}_{\text{cmd}}$ as defined in (50.11).

50.3.2 Steering and Driving Maneuvers

Here, a nonholonomic kinematic model of a four-wheeled mobile robot with each wheel being independently steerable is considered. Figure 50.14 illustrates a two-dimensional kinematic model of the mobile robot having the slip angle of the vehicle β_0 and lateral wheel slippage β_i (the subscript i denotes the wheel identification number, $i = 1, \dots, 4$ in this

case). The dimension of the rover is defined by l_f , l_r , d_R , and d_L . The position and orientation of the vehicle are defined as (x_0, y_0, θ_0) , and the position of each wheel is defined as (x_i, y_i) . In this model, the following assumptions are considered: the distance between the wheels is constant, and the steering axle of each wheel is perpendicular to the terrain surface.

The nonholonomic constraints of the mobile robot are defined by the following equations, with taking the lateral slips of wheels and that of vehicle into account

$$\begin{aligned} \dot{x}_0 \sin \phi_0 - \dot{y}_0 \cos \phi_0 &= 0, \\ \dot{x}_i \sin \phi_i - \dot{y}_i \cos \phi_i &= 0, \end{aligned} \quad (50.12)$$

where $\phi_0 = \theta_0 + \beta_0$ and $\phi_i = \theta_0 + \delta_i + \beta_i$. The geometric constraints between each wheel and the centroid of

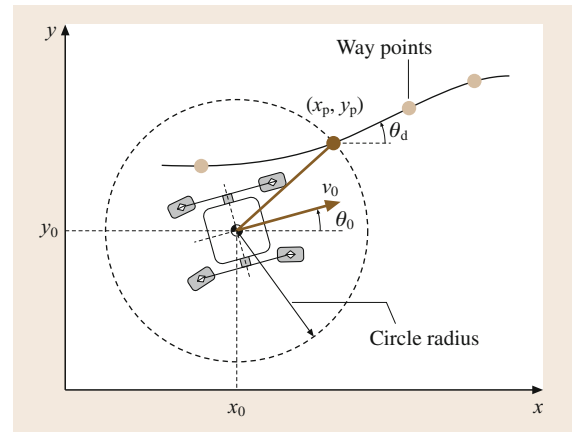


Fig. 50.13 Path following with carrot heading calculation

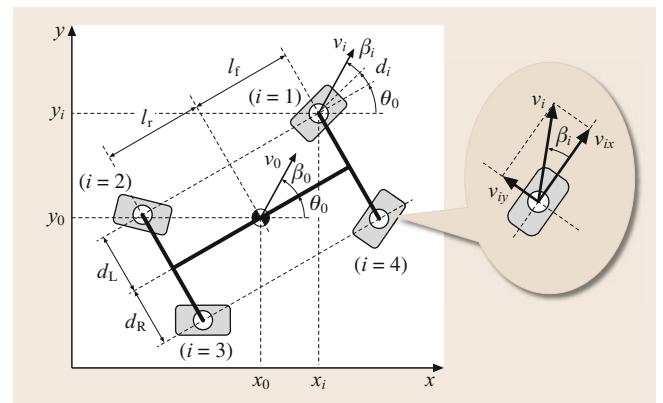


Fig. 50.14 Kinematic model of four-wheeled rover with wheel/vehicle slips

the vehicle are written as

$$\begin{cases} x_1 = x_0 + l_f \cos \theta_0 - d_L \sin \theta_0 \\ x_2 = x_0 - l_r \cos \theta_0 - d_L \sin \theta_0 \\ x_3 = x_0 - l_r \cos \theta_0 + d_R \sin \theta_0 \\ x_4 = x_0 + l_f \cos \theta_0 + d_R \sin \theta_0 \end{cases} \rightarrow x_i = x_0 + X_i, \quad (50.13)$$

$$\begin{cases} y_1 = y_0 + l_f \sin \theta_0 + d_L \cos \theta_0 \\ y_2 = y_0 - l_r \sin \theta_0 + d_L \cos \theta_0 \\ y_3 = y_0 - l_r \sin \theta_0 - d_R \cos \theta_0 \\ y_4 = y_0 + l_f \sin \theta_0 - d_R \cos \theta_0 \end{cases} \rightarrow y_i = y_0 + Y_i. \quad (50.14)$$

Given the desired heading angle $\theta_0 = \theta_d$ and desired linear velocity v_d , the desired steering angle δ_{di} that satisfies the path following control as well as the slip compensation is obtained as follows: first, transform (50.12)

$$\delta_{di} = \tan^{-1} (\dot{y}_i / \dot{x}_i) - \theta_d - \beta_i. \quad (50.15)$$

Subsequently, substituting (50.13) and (50.14) into (50.15), the desired steering angle is determined as follows

$$\delta_{di} = \tan^{-1} \left(\frac{v_d \sin \theta_d - \dot{Y}_i(\dot{\theta}_d)}{v_d \cos \theta_d - \dot{X}_i(\dot{\theta}_{cmd})} \right) - \theta_d - \beta_i. \quad (50.16)$$

The desired yaw rate $\dot{\theta}_{cmd}$ is given from (50.11).

The driving maneuver is practically executed by the wheel angular velocity of the robot. From Fig. 50.14,

the wheel linear velocity v_i is given as

$$v_i = r\omega_i / \cos \beta_i, \quad (50.17)$$

v_i is also expressed by \dot{x}_i or \dot{y}_i

$$v_i = \dot{x}_i / \cos \phi_i = \dot{y}_i / \sin \phi_i. \quad (50.18)$$

Substituting (50.13) or (50.14) into the above equations, the desired wheel angular velocity ω_{di} can be obtained

$$\omega_{di} = \begin{cases} \left(v_d \cos \theta_d + \dot{X}_i(\dot{\theta}_{cmd}) \right) \cos \beta_i / r \cos \phi_i \\ \quad (\theta_d \leq \pi/4), \\ \left(v_d \sin \theta_d + \dot{Y}_i(\dot{\theta}_{cmd}) \right) \cos \beta_i / r \sin \phi_i \\ \quad (\theta_d \geq \pi/4). \end{cases} \quad (50.19)$$

Position and orientation errors relative to a desired path should be accurately determined for deriving the control input as well as calculating the corresponding steering and driving maneuvers. A visual odometry method is of promising technique for such accurate measurement of position, orientation, velocity, and slip-page, and also it is sufficiently robust for loose sandy terrain.

The visual odometry estimates the traveling velocity of the vehicle based on the optical flow vectors obtained from the time-consecutive images taken by an onboard camera(s). Integrating the velocity estimates with inertial measurement unit (IMU) readouts or stereo images for pose estimation provides an accurate estimation of the six degrees of freedom of the rover motion.

50.4 Modeling of Tracked Vehicle on Rough Terrain

Tracks are one of typical mechanism that can enhance the mobility of a robot on rough terrain because they can have contacts between the terrain more widely than wheels. Thus, many types of robots which are required to maneuver rough terrain such as military and search-and-rescue robots have been equipped with tracks.

Some tracked vehicles often have multiple tracks connected by joints to maneuver natural/artificial steps, bumps and stairs. Some are equipped with passive joints, but many are equipped with active joints. Multitracks configuration enables the vehicle to get over a step which is higher than the radius of the tracks.

It should be noted that many tracked vehicles are intended to maneuver the unknown rough terrain con-

sisted of rubbles, rocks, concrete, and woods. Because such types of terrain are nonuniform unlike fine soil discussed in the Sect. 50.2, to dynamically model them is obviously difficult. In other words, we can easily sense the shape of the terrain, but dynamic parameters as well as center of gravity (COG), weight or stiffness of terrain cluster.

Thus, to geometrically consider the interaction between tracks and terrain is a reasonable approach. In this section, a geometrical model of a contact between a track and the terrain surface is introduced. The analysis includes (1) a parameterization of a generic shaped track, (2) contacts between the track and a single point in the terrain surface, and (3) contacts between the track and the terrain surface represented by a point cloud.

50.4.1 Parameterization of a Track

The geometry of a generic-shaped track is the key issue that should be discussed for modeling a tracked vehicle on rough terrain. In this section, we introduce a parameterization of the shape of a generic track.

As shown in Fig. 50.15, a generic track can be parameterized by the radius of the first and the second pulleys, R and r respectively, and the distance between the centers of the pulleys L .

In addition, let us embed the coordinate frame; its origin is at the center of the adjacent track and the x axis is along the center line of the adjacent track. The relative pose of the track respect to the adjacent track can be parameterized by the distance between the origin and the center of the first pulley, and the angle of the joint that connects the tracks θ .

50.4.2 Contact with a Single Point in the Terrain Surface

To discuss contacts between a track and a single point in the terrain surface is a good entrance to understand it between a track and the whole terrain surface. In the following sections, we geometrically describe the former contacts with the parameters of the track defined in the previous section.

As shown in Fig. 50.16, a track generally has four sections that can contact with the terrain surface; since it is tracked, it comprises a round and straight sections. Moreover, it can be in two states, namely, folded and spread states. When the track is in the spread state, side-S supports the robot; on the other hand, when it is in the folded state, side-F is in contact with the terrain. We call the case where side-S is in contact with the ground as the *spreading mode* and the case where side-F is in contact with the ground as the *folding mode*.

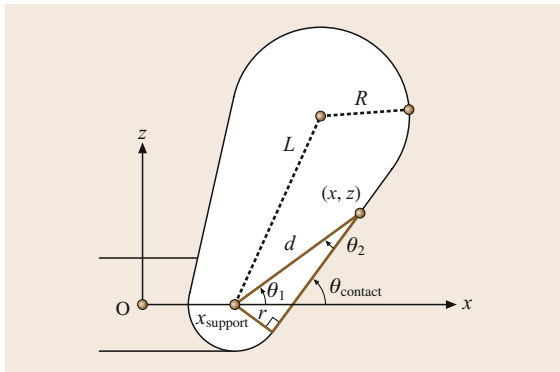


Fig. 50.15 Example of geometrical analysis contact between track and single point on the terrain surface

In addition, we have assumed the pose of the track to be 0° when its straight section on side-S is in contact with the flat surface; we have also assumed the direction in which the track lifts its second pulley from 0° to be positive.

The geometrical relationship between the contact point and pose of the track is summarized in Table 50.1. For example, in the case of the spreading mode and the contact on the straight section (Fig. 50.15), we can derive the following equation according to the geometry of the track contacting with the surface

$$\begin{aligned}\theta_{\text{contact}} &= \theta_1 + \theta_2 \\ &= \tan^{-1} \frac{z}{x - x_{\text{support}}} \\ &\quad + \sin^{-1} \frac{r}{\sqrt{(x - x_{\text{support}})^2 + z^2}}.\end{aligned}\quad (50.20)$$

50.4.3 Contact with the Terrain Surface Represented by a Point Cloud

Now we are well prepared to geometrically understand contacts between the track and the terrain surface. In this section, we describe those contacts by iterating a point cloud that represents the terrain surface.

Let the shape of the terrain surface be represented by a set of points $\{u_1, u_2, \dots, u_n\}$. Then, the contact angle of the track with the surface is determined using the following equation

$$\theta_{\text{ref}} = \begin{cases} \min(\theta_{\text{contact},1}, \dots, \theta_{\text{contact},n}): \\ \text{in spreading mode,} \\ \max(\theta_{\text{contact},1}, \dots, \theta_{\text{contact},n}): \\ \text{in folding mode.} \end{cases}\quad (50.21)$$

To calculate a contact angle of the track with a single point in the terrain surface, we need to determine which section and which side of the track makes the contact.

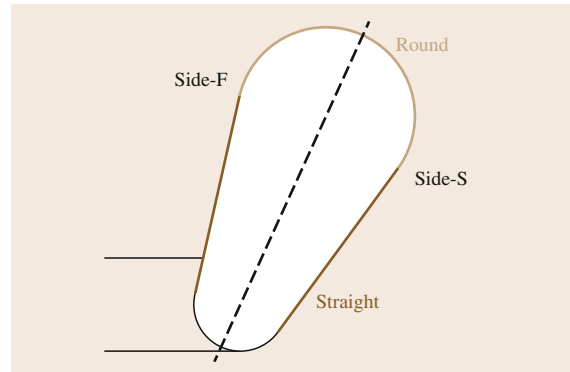


Fig. 50.16 Generic-shaped track consisted of straight and round sections

Table 50.1 Geometric-based contact angle of subtrack

Section		θ_{contact}
Spreading	Straight	$\tan^{-1} \frac{z}{x - x_{\text{support}}} + \sin^{-1} \frac{r}{\sqrt{(x - x_{\text{support}})^2 + z^2}}$
	Round	$\cos^{-1} \frac{d^2 + L^2 - R^2}{2Ld} + \tan^{-1} \frac{z}{x - x_{\text{support}}} - \sin^{-1} \frac{R - r}{L}$
Folding	Straight	$\tan^{-1} \frac{z}{x - x_{\text{support}}} - \sin^{-1} \frac{r}{\sqrt{(x - x_{\text{support}})^2 + z^2}} - 2 \sin^{-1} \frac{R - r}{L}$
	Round	$\tan^{-1} \frac{z}{x - x_{\text{support}}} - \sin^{-1} \frac{R - r}{L} - \cos^{-1} \frac{d^2 + L^2 - R^2}{2Ld}$

The type of the section can be determined by checking the distance between the center of the first pulley and the point; if $d < \sqrt{L^2 + R^2}$ the straight section makes the contact, else the round section does. On the other hand, the side will be determined by the choice of the application.

Now we understand a geometric model which describes contacts between the tracked vehicle consisted of multiple tracks and the free-formed terrain surface whose shape is represented as a point cloud. In the following subsection, we introduce an application example utilizing the contact model.

50.5 Stability Analysis of Tracked Vehicles

As shown in the previous sections, it is hardly possible to build an indentation model of a rough terrain consisted of rubbles. Thus, in this research domain, stability criteria based only on geometrical parameters are often used to evaluate pose of the tracked vehicle on the rough terrain.

This section introduces two typical stability criteria which have been adopted for tracked vehicles; (1)

support polygon and (2) normalized energy stability margin.

The support polygon is a simple and reasonable criterion to determine whether an object on a surface is statically stable. The support polygon for the tracked vehicle is equal to the horizontal projection of the convex hull of all the contact points between the tracks and the terrain. With this support polygon, we can consider

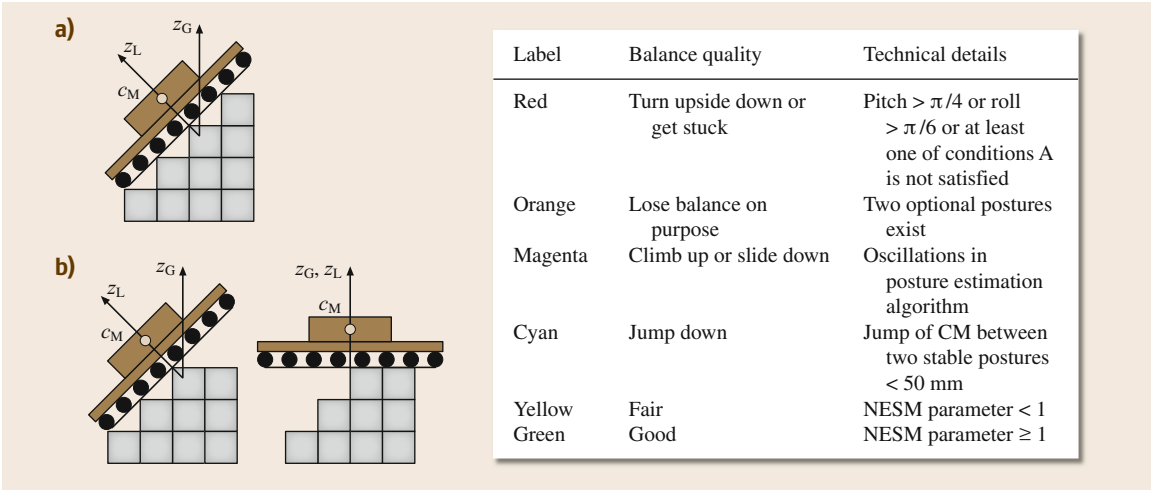


Fig.50.17a,b Example of stability analysis of tracked vehicle on a rough terrain based on support polygon and NESM (after [50.20]); (a) Stable posture corresponding to green label in table. (b) Unstable posture corresponding to orange label in table

that the vehicle is statically stable when it contains the projection of the vehicle's center of gravity.

Another stability criterion is the normalized energy stability margin, or NESM, proposed by Hirose. The NESM is a criterion that is used to evaluate the stability of a robot on the basis of the vertical distance between the initial position of its center of gravity and its highest position during tumbling. Although it is mainly used for walking robots, its evaluation only requires the positions of contact points with the ground and the center of gravity of the robot. In other words, there is no concep-

tual difference if this criterion is applied to the stability of tracked vehicles.

One typical application of stability criteria for the tracked vehicle is to rank possible path in a navigation. For example, Magid proposed a rating method for possible paths based on stability analysis utilizing the support polygon and NESM. This method evaluates the stability of each adjacent grid of the current position of the vehicle; paths to grids on which the support polygon condition is violated are denied. Then survived paths are ranked utilizing the NESM (Fig. 50.17).

50.6 Control of Tracked Vehicle on Rough Terrain

In this section, an approach for the autonomous control of active joints in a tracked vehicle with multiple tracks is introduced. As shown in the previous subsections, the geometric model of the tracked vehicle gives the pose of each track, which makes contact with the rough terrain on the basis of the shape of the terrain surface near the vehicle. The autonomous control utilizes the geometric model to determine the desired angles of the active joints between the tracks to perform a smooth maneuver on an unknown rough terrain.

Tracked vehicles with multiple tracks and joints typically have better locomotion than single-tracked vehicles. This is because one can change the pose of a track by actuating an adequate joint to negotiate bumps or steps in a rough terrain. Some multi-tracked vehicles are equipped with a single-degree-of-freedom (1-DOF) tracked arms, often called subtracks, and the others are snake shaped.

However, multitracked vehicles are difficult to control manually because of their multiple degrees of

freedom. For military and search-and-rescue robots in particular, which are likely to be teleoperated on an unknown rough terrain with limited camera views, it is quite difficult to control all of their DOFs manually.

In the rest of this section, an approach for the autonomous control of active subtracks on the basis of the geometric model of a multitracked vehicle is introduced. In the control algorithm, the geometric model automatically determines the desired poses of active joints, which support subtracks on the basis of the terrain shape obtained in real time.

The multitracked vehicle Kenaf, which has autonomous subtrack control, is shown in Fig. 50.18. Kenaf has two main tracks covering its main body and four subtracks actuated by 1-DOF joints on each corner of the main body. It has 6-DOFs in total: 4-DOFs corresponding to joints supporting the subtracks, 1-DOF corresponding to the one main track and two subtrack belts on the right, and 1-DOF corresponding to the one main track and two subtrack belts on the left.

In addition, Kenaf is equipped with three LIDAR sensors, one on the front, one on the right side, and one on the left side of the main body, to obtain data on the shape of the terrain online. Scans from LIDARs are integrated to estimate the three-dimensional shape of the terrain near the vehicle. The aforementioned approach for autonomous control of active subtracks are described in [50.59].

Figure 50.19 shows the flowchart of the algorithm for the autonomous subtrack control, and its actual motions can be seen in [VIDEO 190](#) and [VIDEO 191](#). The control algorithm is divided into six steps and summarized as follows:

1. Slices of the shape of the terrain around the robot are first obtained from the LIDAR sensors attached

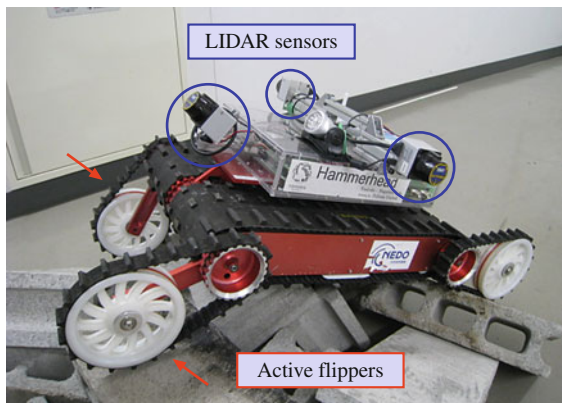


Fig. 50.18 Tracked vehicle Kenaf equipped with four subtracks enhancing mobility and three LIDAR sensors sensing shape of terrain

to the robot body and the three-dimensional terrain shape near the robot is estimated.

2. The desired posture (roll and pitch angles) of the body is then calculated on the basis of the estimated terrain shape.
3. The desired positions of the subtracks that realize the desired posture of the robot body are also determined.
4. Next, the stability of the desired posture and sub-track positions is evaluated.
5. If the desired pose (posture of the robot body and subtrack positions) are unstable, then the desired pose is redefined and steps (3)–(5) are repeated.
6. When the desired subtrack positions that realize a stable posture are generated, position control of the subtracks is finally performed.

In the following sections, we explain each step of the algorithm.

50.6.1 Ground Detection and Trimming of the Scanned Data

In this step, we obtain the scanned points U_{target} near the robot using the LIDAR sensors attached to the robot; ground detection is performed according to the approach described in the paper [50.59]. We first obtain two-dimensional terrain slices from three LIDAR sensors and integrate them according to each tagged and estimated position of the robot to generate the three-dimensional information of the terrain shape. At the end of this step, we filter distant points from the integrated terrain shape.

$$U_{\text{target}} = \{u_1, u_2, \dots, u_m\} \quad (50.22)$$

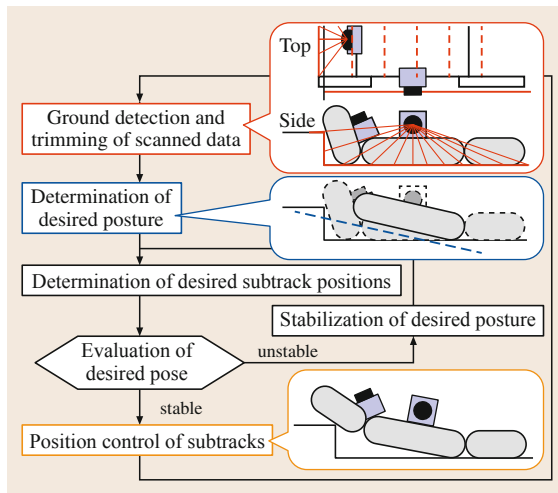


Fig. 50.19 Algorithm for autonomous control of subtracks

50.6.2 Determination of Desired Posture

We then determine the desired posture on the basis of the least-squares plane for the target terrain U_{target} . This is intended to enable smooth locomotion on rough terrain. Parameters a , b , and c of the least-squares plane $z = ax + by + c$ are determined using the following equations (an over-bar indicates the average of m scanned points in U_{target})

$$a = \frac{\alpha_{z,x}\alpha_{y,y} - \alpha_{x,y}\alpha_{y,z}}{\alpha_{x,x}\alpha_{y,y} - \alpha_{x,y}\alpha_{x,y}}, \quad (50.23)$$

$$b = \frac{\alpha_{y,z}\alpha_{x,x} - \alpha_{x,y}\alpha_{z,x}}{\alpha_{x,x}\alpha_{y,y} - \alpha_{x,y}\alpha_{x,y}}, \quad (50.24)$$

$$c = \bar{z}_v - \bar{x}_v a - \bar{y}_v b, \quad (50.25)$$

$$\alpha_{x,y} = \bar{x}_u \cdot \bar{y}_u - \bar{x}_u \cdot \bar{y}_u, \quad (50.26)$$

$$\alpha_{y,z} = \bar{y}_u \cdot \bar{z}_u - \bar{y}_u \cdot \bar{z}_u, \quad (50.27)$$

$$\alpha_{z,x} = \bar{z}_u \cdot \bar{x}_u - \bar{z}_u \cdot \bar{x}_u, \quad (50.28)$$

$$\alpha_{x,x} = \bar{x}_u \cdot \bar{x}_u - \bar{x}_u \cdot \bar{x}_u, \quad (50.29)$$

$$\alpha_{y,y} = \bar{y}_u \cdot \bar{y}_u - \bar{y}_u \cdot \bar{y}_u. \quad (50.30)$$

Then, a translation to the coordinate system, if the robot body is parallel to the least-squares plane of the ground surface and makes contact with the ground, is described by the following equation in quaternion algebra:

$$\begin{pmatrix} 0 \\ x'_{u'_i} \\ y'_{u'_i} \\ z'_{u'_i} \end{pmatrix} = q' \times \begin{pmatrix} 0 \\ x_{u_i} \\ y_{u_i} \\ z_{u_i} \end{pmatrix} \times q'^{-1} - \begin{pmatrix} 0 \\ 0 \\ 0 \\ \max(z_{u'_i}) \end{pmatrix}, \quad (50.31)$$

$$q' = \begin{pmatrix} \cos \frac{\theta_{\text{rot}}}{2} \\ b \sin \frac{\theta_{\text{rot}}}{2} \\ -a \sin \frac{\theta_{\text{rot}}}{2} \\ 0 \end{pmatrix}, \quad (50.32)$$

$$\theta_{\text{rot}} = \cos^{-1} \frac{1}{\sqrt{a^2 + b^2 + 1}}. \quad (50.33)$$

50.6.3 Determination of Desired Subtrack Positions

In this step, using the desired body posture and the integrated terrain slices, we determine the desired subtrack positions on the basis of the geometric model of contacts between the vehicle and the terrain surface.

Our application allows the operator to manually switch between the spreading and the folding control modes. Each control mode employs a corresponding geometric calculation method described in Sect. 50.4. In other words, the autonomous controller uses the corresponding calculation to determine the desired subtrack positions according to the control mode specified by the operator.

In both modes, we determine the desired subtrack positions to make contact with the ground through the desired robot posture. In particular, we calculate the angular position of each subtrack that makes contact with each point scanned by the left and the right LIDAR sensors. The desired position of each subtrack is determined for the maximum or minimum angular position of the subtrack in the spreading or folding mode, respectively.

50.6.4 Stability Evaluation of Desired Pose

In the proposed controller, we have adopted the normalized energy stability margin (NESM) [50.19] as the stability criterion for the desired pose. The stability of a desired pose is evaluated by NESM, and the pose is redefined if the stability is insufficient.

In the case of a tracked vehicle with four subtracks, four contact points (front-right, front-left, rear-right, and rear-left) can be determined by the step described in Sect. 50.6.3. In addition, the four axes of tumbling that pass through the front, rear, right, and left contact points can be assumed. Hence, the stability of a tracked

vehicle with four subtracks can be determined from the minimum value of the NESM about these four axes.

50.6.5 Stabilization of Desired Pose

When the NESM of the robot is less than a predetermined threshold, we repeat the following steps until a desired, stable pose is realized. This step is intended to realize the strategy 4:

- 1a. If the NESM about the front or rear is adopted, reduce the pitch angle of the desired posture to zero.
- 1b. When the NESM about the right or left is adopted, reduce the roll angle of the desired posture to zero.
2. Redefine the desired subtrack positions by recalculating them to realize the redefined desired posture.
3. Evaluate the NESM about the redefined posture and positions of subtracks.

50.6.6 Position Control of Subtracks

Finally, we perform position control of the subtracks to realize the desired subtrack position produced through the above-mentioned steps on the basis of the strategy described in the previous subsection.



All subtracks of Kenaf and Quince are controlled by microprocessors present on the built-in motor drivers. Each desired subtrack position is sent to the corresponding microprocessor as a reference for position control using the conventional proportional–integral–derivative (PID) controller.







50.7 Summary

In this chapter, an overview of the modeling and control of robots on the rough terrain motion has been provided. The target environment was rough terrains, which includes a variety of ground conditions. In the case of weak and fine gravel, the motion of a wheeled mobile robot becomes relatively complicated because the interaction mechanics of the wheel in rough terrains differs greatly from that of an indoor robot on a flat surface. In this chapter, we introduced a terramechanics-

based model for the interactions between wheels and deformable terrains. Furthermore, we explained the steering control of wheeled mobile robots to enable path-following in such environments. In the case of an environment with heaps of rubble, the approach for controlling robots is different from the terramechanics approach. Therefore, we introduced an initial attempt at a sensor-based approach that involved measuring the terrain shape.

Video-References

-  **VIDEO 184** Mobility prediction of rovers on soft terrain available from <http://handbookofrobotics.org/view-chapter/50/videodetails/184>
-  **VIDEO 185** Experiments of wheeled rovers in a sandbox covered with loose soil available from <http://handbookofrobotics.org/view-chapter/50/videodetails/185>

-  VIDEO 186 Terradynamics of legged locomotion for traversal in granular media available from <http://handbookofrobotics.org/view-chapter/50/videodetails/186>
-  VIDEO 187 Interaction human-robot supervision, long range science rover for Mars exploration available from <http://handbookofrobotics.org/view-chapter/50/videodetails/187>
-  VIDEO 188 A path-following control scheme for a four-wheeled mobile robot available from <http://handbookofrobotics.org/view-chapter/50/videodetails/188>
-  VIDEO 189 Evaluation test of tracked vehicles on random step fields in the Disaster City available from <http://handbookofrobotics.org/view-chapter/50/videodetails/189>
-  VIDEO 190 Autonomous sub-tracks control available from <http://handbookofrobotics.org/view-chapter/50/videodetails/190>
-  VIDEO 191 Autonomous sub-tracks control available from <http://handbookofrobotics.org/view-chapter/50/videodetails/191>

References

- 50.1 M. Jurkat, C. Nuttall, P. Haley: *The AMC' 74 Mobility Model, Tech. Rep. 11921* (US Army Tank Automotive Command, Warren, 1975)
- 50.2 R.B. Ahlvin, P.W. Haley: *NATO Reference Mobility Model Edition II, NRMM User's Guide, Tech. Rep. GL-92-19* (US Army WES, Vicksburg, 1992)
- 50.3 A. Gibbesch, B. Schäfer: Multibody system modelling and simulation of planetary rover mobility on soft terrain, 8th Int. Symp. Artif. Intell. Robotics Autom. Space (i-SAIRAS), Munich (2005)
- 50.4 R. Krenn, A. Gibbesch, G. Hirzinger: Contact dynamics simulation of rover locomotion, Proc. 9th Int. Symp. on Artif. Intell., Robotics Autom. Space, Los Angeles (2007)
- 50.5 D. Holz, A. Azimi, M. Teichmann, J. Kövecses: Mobility prediction of rovers on soft terrain: Effects of wheel- and tool-induced terrain deformations, Proc. 15th Int. Conf. Climbing Walk. Robots Support Technol. Mob. Mach. (CLAWAR) (2012)
- 50.6 J.Y. Wong: *Theory of Ground Vehicles* (Wiley, New York 1978)
- 50.7 M. Buehler, K. Iagnemma, S. Singh (Eds.): *The 2005 DARPA Grand Challenge: The Great Robot Race Springer Tracts Adv. Robotics Ser.*, Vol. 36 (Springer, Berlin, Heidelberg 2005)
- 50.8 M. Buehler, K. Iagnemma, S. Singh (Eds.): *The DARPA Urban Challenge: Autonomous Vehicles in City Traffic*, Springer Tracts Adv. Robotics, Vol. 56 (Springer, Berlin, Heidelberg 2009)
- 50.9 C. Li, T. Zhang, D.I. Goldman: A terradynamics of legged locomotion on granular media, *Science* **339**, 1408–1412 (2013)
- 50.10 C. de Wit, H. Khenouf, C. Samson, O. Sordalen: Nonlinear control design for mobile robots. In: *Recent Trends in Mobile Robots*, World Scientific Series in Robotics and Automated System, Vol. 11, ed. by Y. Zheng (World Scientific, Singapore 1993)
- 50.11 A. Luca, G. Oriolo, C. Samson: Feedback control of nonholonomic car-like robots. In: *Robot Motion Planning and Control*, ed. by J. Laumond (Springer, Berlin, Heidelberg 1998) pp. 171–254
- 50.12 F. Rio, G. Jimenez, J. Sevillano, S. Vicente, A. Balcells: A generalization of path following for mobile robots, Proc. 1999 IEEE Int. Conf. Robotics Autom. (ICRA), Detroit (1999) pp. 7–12
- 50.13 S. Rezaei, J. Guivant, E. Nebot: Car-like robot path following in large unstructured environments, Proc. IEEE Int. Conf. Intell. Robots Syst. (IROS) (2003) pp. 2468–2473
- 50.14 P. Coelho, U. Nunes: Path-following control of mobile robots in presence of uncertainties, *IEEE Trans. Robotics* **21**(2), 252–261 (2005)
- 50.15 D. Helmick, Y. Cheng, D. Clouse, L. Matthies, S. Roumeliotis: Path following using visual odometry for a Mars rover in high-slip environments, Proc. 2004 IEEE Aerosp. Conf., Big Sky (2004) pp. 772–789
- 50.16 D. Helmick, S. Roumeliotis, Y. Cheng, D. Clouse, M. Bajracharya, L. Matthies: Slip-compensated path following for planetary exploration rovers, *Adv. Robotics* **20**(11), 1257–1280 (2006)
- 50.17 G. Ishigami, K. Nagatani, K. Yoshida: Slope traversal controls for planetary exploration rover on sandy terrain, *J. Field Robotics* **26**(3), 264–286 (2009)
- 50.18 D.A. Messuri, C.A. Klein: Automatic body regulation for maintaining stability of a legged vehicle during rough-terrain locomotion, *IEEE J. Robotics Autom.* **1**(3), 132–141 (1985)
- 50.19 S. Hirose, H. Tsukagoshi, K. Yoneda: Normalized energy stability margin and its contour of walking vehicles on rough terrain, Proc. IEEE Int. Conf. Robotics Autom. (ICRA) (2001) pp. 181–186
- 50.20 E. Magid, T. Tsubouchi, E. Koyanagi, T. Yoshida, S. Tadokoro: Controlled balance losing in random step environment for path planning of a teleoperated crawler-type vehicle, *J. Field Robotics* **28**(6), 932–949 (2011)
- 50.21 A. Jacoff, E. Messina, B.A. Weiss, S. Tadokoro, Y. Nakagawa: Test arenas and performance metrics for urban search and rescue robots, Proc. IEEE/RSJ Int. Conf. Intell. Robots Syst. (IROS), Las Vegas (2003) pp. 3396–3403
- 50.22 K. Ohno, V. Chun, T. Yuzawa, E. Takeuchi, S. Tadokoro, T. Yoshida, E. Koyanagi: Rollover avoidance using a stability margin for a tracked vehicle with sub-tracks, IEEE Int. Workshop Saf. Sec. Rescue Robotics (2009)
- 50.23 N. Vandapel, D. Huber, A. Kapuria, M. Hebert: Natural terrain classification using 3-D ladar data, Proc. IEEE Int. Conf. Robotics Autom. (ICRA), Vol. 5 (2004) pp. 5117–5122

- 50.24 M. Onosato, S. Yamamoto, M. Kawajiri, F. Tanaka: Digital gareki archives: An approach to know more about collapsed houses for supporting search and rescue activities, IEEE Int. Symp. Saf. Secur. Rescue Robotics (SSRR) (2012) pp. 1–6
- 50.25 A. Lacaze, K. Murphy, M. Del Giorno: Autonomous mobility for the demo III experimental unmanned vehicles, AUVS Int. Conf. Unmanned Veh. (2002)
- 50.26 K. Ohno, T. Suzuki, K. Higashi, M. Tsubota, E. Takeuchi, S. Tadokoro: Classification of 3-D point cloud data that includes line and frame objects on the basis of geometrical features and the pass rate of laser rays, Proc. 8th Int. Conf. Field Serv. Robotics (2012)
- 50.27 M. Onosato, T. Watasue: Two attempts at linking robots with disaster information: InfoBalloon and gareki engineering, Adv. Robotics **16**(6), 545–548 (2002)
- 50.28 M. Onosato: Digital GAREKI modeling for exploring knowledge of disaster-collapsed houses, IEEE Int. Workshop Saf. Secur. Rescue Robotics (SSRR) (2006)
- 50.29 L. Woosub, K. Sungchul, K. Munsang, P. Mignon: ROBHAZ-DT3: Teleoperated mobile platform with passively adaptive double-track for hazardous environment applications, Proc. IEEE/RSJ Int. Conf. Intell. Robots Syst. (IROS) (2004) pp. 33–38
- 50.30 B. Yamauchi: Packbot: A versatile platform for military robotics, Proc. SPIE **5422**, 228–237 (2004)
- 50.31 D. Inoue, K. Ohno, S. Nakamura, S. Tadokoro, E. Koyanagi: Whole-body touch sensors for tracked mobile robots using force-sensitive chain guides, IEEE Int. Workshop Saf. Secur. Rescue Robotics (SSRR) (2008) pp. 71–76
- 50.32 A. Jain, J. Balaram, J. Cameron, J. Guineau, C. Lim, M. Pornerantz, G. Sohl: Recent developments in the ROAMS planetary rover simulation environment, Proc. 2004 IEEE Aerosp. Conf., Big Sky (2004) pp. 861–876
- 50.33 K. Iagnemma, C. Senatore, B. Trease, R. Arvidson, A. Shaw, F. Zhou, L. Van Dyke, R. Lindemann: Terramechanics modeling of mars surface exploration rovers for simulation and parameter estimation, ASME Int. Des. Eng. Tech. Conf. (2011)
- 50.34 R. Bauer, W. Leung, T. Barfoot: Development of a dynamic simulation tool for the exomars rover, Proc. 8th Int. Symp. Artif. Intell., Robotics Autom. Space, Munich (2005)
- 50.35 M.G. Bekker: *Theory of Land Locomotion* (Univ. Michigan Press, Ann Arbor 1956)
- 50.36 M.G. Bekker: *Introduction to Terrain-Vehicle Systems* (Univ. Michigan Press, Ann Arbor 1969)
- 50.37 J.Y. Wong: *Theory of Ground Vehicles*, 4th edn. (Wiley, Hoboken 2008)
- 50.38 J.Y. Wong, A.R. Reece: Prediction of rigid wheel performance based on the analysis of soil-wheel stresses – Part I: Performance of driven rigid wheels, J. Terramechanics **4**(1), 81–98 (1967)
- 50.39 J.Y. Wong, A.R. Reece: Prediction of rigid wheel performance based on the analysis of soil-wheel stresses – Part II: Performance of towed rigid wheels, J. Terramechanics **4**(2), 7–25 (1967)
- 50.40 I.C. Schmid: Interaction of vehicle and terrain results from 10 years research at IKK, J. Terramechanics **32**(1), 3–25 (1995)
- 50.41 L. Ding, Z. Deng, H. Gao, K. Nagatani, K. Yoshida: Planetary rovers' wheel-soil interaction mechanics: New challenges and applications for wheeled mobile robots, Intell. Serv. Robotics **4**(1), 17–38 (2010)
- 50.42 H. Nakashima, H. Fujii, A. Oida, M. Momozu, Y. Kawase, H. Kanamori, S. Aoki, T. Yokoyama: Parametric analysis of lugged wheel performance for a lunar microrover by means of DEM, J. Terramechanics **44**, 153–162 (2007)
- 50.43 H. Nakashima, H. Fujii, A. Oida, M. Momozu, H. Kanamori, S. Aoki, T. Yokoyama, H. Shimizu, J. Miyasaka, K. Ohdoi: Discrete element method analysis of single wheel performance for a small lunar rover on sloped terrain, J. Terramechanics **47**, 307–321 (2010)
- 50.44 W. Li, Y. Huang, Y. Cui, S. Dong, J. Wang: Trafficability analysis of lunar mare terrain by means of the discrete element method for wheeled rover locomotion, J. Terramechanics **47**, 161–172 (2010)
- 50.45 K. Iagnemma: *A Laboratory single wheel testbed for studying planetary rover wheel-terrain interaction*, Tech. Rep. 01-05-05 (MIT, Cambridge 2005)
- 50.46 S. Wakabayashi, H. Sato, S. Nishida: Design and mobility evaluation of tracked lunar vehicle, J. Terramechanics **46**(3), 105–114 (2009)
- 50.47 N. Patel, R. Slade, J. Clemmet: The ExoMars rover locomotion subsystem, J. Terramechanics **47**, 227–242 (2010)
- 50.48 G. Ishigami, A. Miwa, K. Nagatani, K. Yoshida: Terramechanics-based model for steering maneuver of planetary exploration rovers on loose soil, J. Field Robotics **24**(3), 233–250 (2007)
- 50.49 R. Lindemann, D. Bickler, B. Harrington, G. Ortiz, C. Voorhees: Mars exploration rover mobility development, IEEE Robotics Autom. Mag. **13**(2), 19–26 (2006)
- 50.50 G. Ishigami, A. Miwa, K. Nagatani, K. Yoshida: Terramechanics-based analysis on slope traversability for a planetary exploration rover, Proc. 25th Int. Symp. Space Technol. Sci. (2006) pp. 1025–1030
- 50.51 S. Michaud, L. Richter, T. Thueer, A. Gibbesch, T. Huelsing, N. Schmitz, S. Weiss, A. Krebs, N. Patel, L. Joudrier, R. Siegwart, B. Schäfer, A. Ellery: Rover chassis evaluation and design optimisation using the RCET, Proc. 9th ESA Workshop Adv. Space Technol. Robotics Autom. (ASTRA) (2006)
- 50.52 K. Nagatani, A. Ikeda, K. Sato, K. Yoshida: Accurate estimation of drawbar pull of wheeled mobile robots traversing sandy terrain using built-in force sensor array wheel, Proc. 2009 IEEE/RSJ Int. Conf. Robots Syst. (IROS), St. Louis (2009) pp. 2373–2378
- 50.53 G. Meirion-Griffith, M. Spenko: A Modified pressure-sinkage model for small, rigid wheels on deformable terrains, J. Terramechanics **48**(2), 149–155 (2011)
- 50.54 C. Senatore, K. Iagnemma: Direct shear behaviour of dry, granular soils for low normal stress with

application to lightweight robotic vehicle modeling, 17th Conf. Terrain-Veh. Syst. (ISTVS), Blacksburg (2011)

50.55 K. Iagnemma, S. Kang, H. Shibly, S. Dubowsky: Online terrain parameter estimation for wheeled mobile robots with application to planetary rovers, *IEEE Trans. Robotics* **20**(5), 921–927 (2004)

50.56 S. Hutangkabodee, Y. Zweiri, L. Seneviratne, K. Althoefer: Soil parameter identification for wheel-terrain interaction dynamics and traversability prediction, *Int. J. Autom. Comput.* **3**(3), 244–251 (2006)

50.57 D. Helmick, A. Angelova, L. Matthies, C. Brooks, I. Halatci, S. Dubowsky, K. Iagnemma: Experimental results from a terrain adaptive navigation system for planetary rovers, *Proc. 9th Int. Symp. Artif. Intell., Robotics Autom. Space (i-SAIRAS)*, Hollywood (2008)

50.58 G. Ishigami, G. Kewlani, K. Iagnemma: A statistical approach to mobility prediction for planetary surface exploration rovers in uncertain terrain, *IEEE Robotics Autom. Mag.* **16**(4), 61–70 (2009)

50.59 O. Yoshito, K. Nagatani, K. Yoshida, S. Tadokoro, T. Yoshida, E. Koyanagi: Shared autonomy system for traversing and turning tracked vehicles on rough terrain based on continuous three-dimensional terrain scanning, *J. Field Robotics* **28**(6), 875–893 (2011)